Institute of Paper Science and Technology
Atlanta, Georgia

IPST TECHNICAL PAPER SERIES

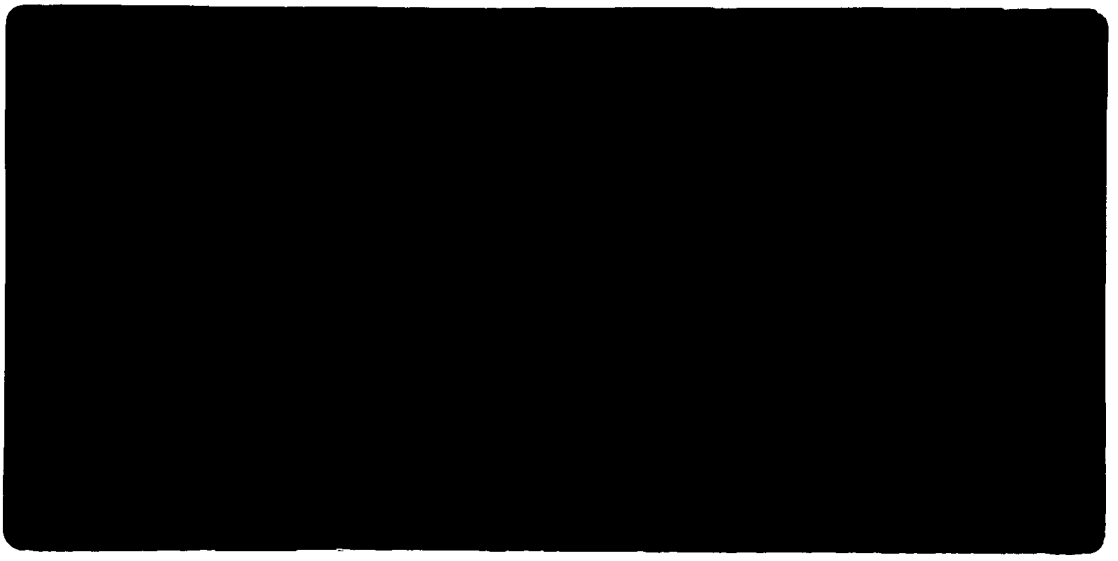

NUMBER 478

CFD SIMULATIONS OF RECOVERY BOILER CHAR BEDS WITH STEP AND SMOOTH SURFACES

W. YANG, R.R. HORTON, AND T.N. ADAMS

APRIL 1993

CFD Simulations of Recovery Boiler Char Beds with Step and Smooth Surfaces

W. Yang, R.R. Horton, and T.N. Adams

Submitted to
Tappi Journal

CFD SIMULATIONS OF RECOVERY BOILER CHAR BEDS WITH STEP AND SMOOTH SURFACES

Wenrui Yang, Robert R. Horton, and Terry N. Adams

ABSTRACT

Step boundaries have often been used to approximate smooth boundaries in CFD simulations with orthogonal Cartesian coordinate grids. This paper investigates the use of steps to represent a smooth sloped surface that is typical of recovery furnace char beds. In this work the lower region of a recovery furnace was simulated with CFD models, and the slope of the char bed was represented by either a Cartesian coordinate step surface or a body-fitted-coordinate smooth surface. The effects of a step boundary on the calculations of gas velocity, shear stress, and heat transfer coefficient on the bed surface were then examined. Results showed that both methods predicted similar overall velocity fields, but the step-bed model underestimated shear stress and overestimated heat transfer area at the surface boundary. Moreover, the step-bed model was numerically less stable and converged slower than the smooth-bed model. Smooth boundaries are strongly recommended when the transport processes at the surface need to be predicted accurately.

INTRODUCTION

Computational Fluid Dynamics (CFD) is a powerful tool for studying complicated flow fields and transport processes. One of the most challenging problems posed for CFD study is the simulation of recovery furnaces. The extremely hostile environment in an operating furnace makes it a formidable task to measure velocities and transport processes, yet the information is important for understanding and improving furnace performance. Physical models have been useful for simulating flow at room temperatures (1-3), but it is difficult to include the heat transfer and chemical reactions that occur in an operating furnace. CFD simulation offers an attractive alternative for analyzing and understanding recovery boiler operation.

Recovery furnaces involve complicated chemical and physical processes. With some simplifications, CFD simulations have been successfully used to study the gas flow patterns (3-14), temperature distributions (5, 6, 8, 14, 15), and trajectories of black liquor particles (6, 14, 16). The results have increased our understanding of combustion behavior in the furnaces. The interaction between char bed and gas flow is another area in which CFD techniques can be used to analyze recovery boiler operation; however, little work has been done in this area.

Char bed combustion is important for stable operation of recovery boilers. The bed shape directly affects the gas flow pattern since the primary and secondary air jets are deflected by the bed surface (4, 5). In turn, the gas flow affects the bed shape by influencing black liquor arrival patterns and heat and mass transfer rates on the bed surface. Stable operation is achieved when arrival of black liquor matches consumption. Changes in the gas flow pattern could result in an unstable bed shape.

The large size of typical furnace combustion zones relative to the small features, such as primary air ports, adds another difficulty to CFD modeling (4, 14). For example, an entire furnace model with 200,000 nodes would merely resolve the major flow features, such

as secondary and tertiary jet penetration and large recirculation zones, but primary jets could only be represented by one node (14). Models with less than 50,000 nodes for one half of a furnace would have to use slots as primary air ports (4, 16). To study the interaction between air jets and the char bed, it is essential to describe the bed shape accurately. To reduce computational burden and increase accuracy for small flow features, a section of the furnace can be simulated independently by assuming proper boundary conditions to isolate it from the rest of the furnace (4, 8, 16, 17).

In some commercial CFD codes, computational grids can be set up in either Cartesian coordinates or body-fitted-coordinates (BFC). Grids in Cartesian coordinates consist of orthogonal grid lines. If a boundary is not aligned to one of the grid lines, a series of steps must be used to approximate the real boundary. The error caused by the step boundary may seriously affect calculations of flow fields if the step size is comparable to the sizes of flow features (4). Even with small steps, which do not have serious influence on the gas flow patterns, the calculations of the transport processes on the surface may be in error. In BFC grids, the grid lines do not need to be orthogonal and can be aligned to boundaries so that the boundaries are smooth regardless of orientation (18). In addition, internal grid lines of BFC grids can be manipulated to follow major flow features, reducing errors caused by numerical diffusion (19). In general, a BFC grid is more accurate than a Cartesian grid for irregular boundaries, but it may not be available in all CFD codes.

This paper presents a two-dimensional CFD study on jet flows near a char bed in a recovery furnace, with special attention paid to the effects of the char bed boundary, which is represented either by a series of steps or by a smooth surface, on gas velocity, shear stress, and heat transfer rate. To reveal details on the bed surface, the computational domain was focused in a small zone of the lower furnace.

DESCRIPTION OF CHAR BED MODELS

Two-dimensional, isothermal models are used in this work to examine the differences between step and smooth boundaries for the char bed. Figures 1 and 2 show the geometry and grids of the two models. The char bed and the flow field are assumed to be symmetrical to the centerline of the furnace, so only half of the char bed and furnace domain is included in the models. The domain is 5 m from the wall to the center (x direction) and 4 m from base to top (y direction). The bed surface starts to rise at 0.15 m from the wall with a 1:2 slope, and levels off 3.7 m from the wall. The height of the bed in the center of the furnace is 1.775 m. A 0.3 m primary air port is located on the wall at an elevation of 0.05 m, and a 0.5 m secondary air port is located at an elevation of 1.5 m. The grid lines are non-uniformly distributed to achieve higher resolutions near the air ports. Primary air velocity is 50 m/s in a 10° downward angle, and secondary air velocity is 80 m/s in the horizontal direction. An isothermal condition is assumed, and the physical properties of air at 1000 °C are used.

A Cartesian coordinate grid and a BFC grid are compared in this study. In the Cartesian coordinate grid, the char bed surface consists of steps because the sloped surface is not aligned to the orthogonal grid lines (Figure 1). In the BFC model, the grid lines are aligned with the boundaries, and the char bed has a smooth surface (Figure 2). The numbers of grid lines are the same in both cases (62×80).

In both models, nonslip wall boundary conditions are used for the wall and the bed; a symmetry boundary condition is used for the center line; fixed velocity inlets are used for the air ports; and a fixed pressure boundary condition is used for the upper boundary. The standard κ-ϵ turbulence model is used. The simulations were carried out on an IBM RISC/6000 computer with FLUENT version 4.11 (18, 19).

RESULTS AND DISCUSSION

Flow Field

The velocity distributions for the step bed and the smooth bed are shown in Figures 3 and 4. The major flow features in both models, such as air jets and recirculation zones, are similar; however, the gas flow near the step surface is disturbed. The disturbance on the overall flow pattern is so small that it can be neglected for the purpose of predicting velocities in the bulk gas phase. Figure 5 compares velocity profiles along a vertical line in the middle of the simulation region (x = 2.5 m). The horizontal and vertical velocity components, v_x and v_y, are shown separately. In the bulk gas phase, the velocity profiles are very similar; however, there are significant differences near the bed surface, where the step-bed model predicts much lower velocity than the smooth-bed model.

Shear Stress on Bed Surface

Although the influence of steps on velocity is restricted to a very small region near the char bed, it significantly affects the calculation of shear stress on the bed surface. Figure 6 shows distribution of the x component of the shear stress, $(\tau_w)_x$, on the step and smooth bed surfaces. For the smooth bed, the shear stress distribution pattern has a maximum produced by the impingement of the primary air, whereas for the step bed, the shear stress has a different pattern with smaller values but larger fluctuations. The average error for the shear stress on the step bed is 62% based on the shear stress of the smooth bed.

The major difference in shear stress between the step and smooth beds is caused by the velocity difference near the bed surface. In turbulent flows, a wall boundary layer consists of a very thin laminar sublayer and a "log-law" region in which the flow is fully turbulent. The first node near the wall should be within the log-law region, and the wall shear stress is calculated via the log-law wall function (19, 20):

$$\frac{u_p}{u^*} = \frac{1}{\kappa}\ln(Ey^+), \tag{1}$$

where $u^* = \sqrt{\tau_w/\rho}$ is called the *friction velocity*; τ_w is the wall shear stress; u_p is the gas velocity at the first node (point p) near the surface; κ is von Karman's constant (= 0.42); E is an empirical constant (= 9.81 for a smooth wall); and y^+ is defined by

$$y^+ = \rho u^* y/\mu, \tag{2}$$

where y is the distance from point p to the wall. Upon using the boundary condition for the turbulent kinetic energy:

$$k_p = u^{*2}/\sqrt{C_\mu}, \tag{3}$$

Equation (2) becomes

$$y^+ = \frac{\rho k_p^{1/2} C_\mu^{1/4} y}{\mu}, \tag{4}$$

where k_p is the turbulent kinetic energy at point p, and C_μ is an empirical constant (= 0.09). Equation (1) implies that u^* is proportional to u_p, i.e., τ_w is proportional to u_p^2 if y^+ is constant. This means that the shear stress is very sensitive to the gas velocity near the wall.

In the smooth-bed model, the boundary grid lines exactly follow the char bed surface, and the calculations can be correctly carried out for the nodes adjacent to the surface. The resulting velocity distribution is smooth and consistent, as shown in Figure 7 for the velocity vectors. In the step-bed model, the step surface deviates from the real surface. Beyond a

short distance above the bed surface, the step effect is negligible, and the gas velocity is correctly calculated. However, at nodes adjacent to the surface, velocity tends to follow the step contour, which is misleading for the local gas flow, as shown in Figure 8. Nodes located at the corners of the steps are partially blocked by wall surfaces that do not exist on the true surface; consequently, the velocity near the surface is underestimated, resulting in erroneous shear stress predictions. Notice that, in Figure 8, one of the steps faces two horizontal nodes, causing a variation in predicted velocity. Such a variation in velocity results in a spike-like pattern in the shear stress distribution (see Figure 6).

The region of highest computational error in the step-boundary model is the same order of magnitude as the step size. As the step size decreases, the region of error becomes smaller, and the gas flow pattern approaches that of a smooth bed; however, the error of the shear stress is not reduced in a similar fashion. As Equations (1) and (2) indicate, only the adjacent nodes are used in the calculations of the shear stress. No matter how small the steps are, the nodes at the corners of the steps are similarly blocked by the wall surfaces, causing the velocity to be underestimated. If the nodes are so close to the bed surface that they are within the laminar sublayer ($y^+ < 11.6$), the laminar boundary equation, i.e., $u/u^* = y^+$, instead of Equation (1), will be used. This is not recommended for turbulent flows. In all the simulations in this study, y^+ is well above the limit for the laminar sublayer.

Implications on Heat and Mass Transfer Rates

Shear stress can be used to predict heat and mass transfer rates on the bed surface (17, 19, 20, 21). For this reason, shear stress prediction has important implications. For turbulent flows, the heat transfer to the wall is calculated by a log-law formulation that is based on the analogy between heat and momentum transfer (19, 20):

$$\frac{k_f/y}{q''/\Delta T} = \frac{1}{\kappa y^+}\frac{Pr_t}{Pr}\ln(Ey^+) + \frac{\pi/4}{\sin(\pi/4)y^+}\left(\frac{A}{\kappa}\right)^{1/2}\left(\frac{Pr_t}{Pr}\right)^{5/4}\left(\frac{Pr}{Pr_t} - 1\right), \quad (5)$$

where k_f is the thermal conductivity of the fluid; q'' is the wall heat flux; $\Delta T = T_w - T_f$ is the local temperature difference between the wall and the fluid; Pr is the molecular Prandtl number; Pr_t is the turbulent Prandtl number (= 1.2 in the log-law region); and A is the van Driest constant (= 26). Notice that the first term on the right-hand side of Equation (5) is similar to that of Equation (1), and velocity (u_p) is not included in the equation. The heat transfer coefficient depends on the turbulent kinetic energy and temperature, which determine y^+ and physical properties.

To study the effects of the step boundary on the heat transfer calculations, we included heat transfer calculations in another series of simulations, with the char bed and the wall having constant temperatures of 800 °C and the inlet air set at 100 °C. Radiation heat transfer and heat generation by combustion were not included. The smooth-bed model converged easily (sum of residuals $< 10^{-3}$ and enthalpy residual $< 10^{-6}$) in 3900 iterations (6.7 hours CPU time), but the step-bed model reached a stable solution with a large enthalpy residual (4×10^{-3}) after 50,000 iterations (60 hours CPU time).

As shown in Figure 9, the shear stress distribution patterns are very similar to those for the isothermal cases, but the values are approximately twice as large because the gas density is larger at lower temperatures in this case. The average error for the shear stress on the step bed is 64% based on the smooth-bed model. The CFD code used in this study calculates the heat transfer coefficient using the wall heat flux and temperature difference between wall temperature and volumetric bulk average fluid temperature in the computational domain:

$$h = \frac{q''}{T_w - \bar{T}_b}, \quad (6)$$

where h is heat transfer coefficient, and $\bar{T}_b$ is the volumetric bulk average fluid temperature. When the wall temperature is constant, as is in this case, the heat transfer coefficient is proportional to the wall heat flux.

Figure 10 compares the heat transfer coefficients on the step and smooth surfaces. The heat transfer coefficients in the two cases are comparable except in the area impinged by the primary air jet, even though the shear stresses have large differences. The average error for the heat transfer coefficient on the step surface is 14% based on the smooth-bed model, compared with 64% for the shear stress. Equation (5) indicates that the most influential variables for the heat transfer coefficient are turbulence kinetic energy and temperature. We noticed that the difference between the turbulent kinetic energies near the step and smooth surfaces was smaller than that between the corresponding shear stresses, but this does not imply that the step-bed model is suitable for heat transfer calculations. As Table 1 shows, the heat transfer area of the step bed is 26% larger than that of the smooth bed; consequently, the overall heat transfer rate of the step bed is 23% larger than that of the smooth bed.

Table 1. Heat transfer on the step and smooth beds.

	Step bed	Smooth bed
Heat transfer area (m^2)	6.8	5.4
Average heat flux (W/m^2)	4.7×10^4	4.9×10^4
Overall heat rate (W)	3.2×10^5	2.6×10^5

CONCLUSIONS

This paper presents results of CFD simulations on recovery furnace char beds with step or smooth boundaries for the bed surface. The smooth boundary has been found to represent the actual bed geometry more accurately. The step-bed model gives satisfactory results for the bulk gas flow patterns, but the deviation of the step surface from the true surface causes errors in two aspects: (1) the disturbance of velocity near the steps results in large errors in shear stress and heat transfer coefficient, and (2) miscalculation of the surface area leads to an error in total heat transfer rate. Additionally, the step-bed model is numerically less stable and converges slower than the smooth-bed model. Therefore, the smooth body-fitted-coordinate boundary is superior to the step Cartesian coordinate boundary in both accuracy and speed of convergence.

ACKNOWLEDGEMENT

This work was supported by DOE under contract No. DE-FG02-90CE40936.

NOMENCLATURE

A = 26, van Driest constant

C_μ = 0.09, empirical constant

E = 9.81, empirical constant

h heat transfer coefficient, W/(m^2.K)

k turbulent kinetic energy, (m/s)^2

k_f thermal conductivity of fluid, W/(m.K)

Pr Prandtl number

Pr_t turbulent Prandtl number

$q"$ wall heat flux, W/m^2

u velocity magnitude, m/s

u^* $= \sqrt{\tau_w/\rho}$, friction velocity, m/s

T_w wall temperature, K

T_f gas temperature, K

$\bar{T}_b$ volumetric bulk average gas temperature, K

y distance from the first node to the wall, m

y^+ dimensionless variable defined by Equation (2)

μ viscosity, kg/(m.s)

ρ density, kg/m^3

κ $= 0.42$, von Karman's constant

τ_w wall shear stress, Pa

REFERENCES

1. Ketler, S. P., Savage, M. C., and Gartshore, I. S., "Physical Modeling of Flow in Black Liquor Recovery Boilers," *Proc. TAPPI Eng. Conf.*, p. 581, 1992.

2. Llinares, V., Jr. and Chapman, P. J., "Combustion Engineering Update Stationary Firing, Three Level Air System Retrofit Experience," *Proc. TAPPI Eng. Conf.*, p. 629, 1989.

3. Chapman, P. J. and Jones, A. K., "Recovery Boiler Secondary Air System Development Using Experimental and Computational Fluid Dynamics," *Proc. TAPPI Eng. Conf.*, p. 193, 1990.

4. Jones, A. K. and Grace T. M., "A Comparison of Computational and Experimental Methods for Determining the Gas Flow Patterns in the Kraft Recovery Boiler," *Proc. TAPPI Eng. Conf.*, p. 3, 1988.

5. Sumnicht, D. W., "A Computer Model of a Kraft Char Bed," Ph.D. Thesis, IPC, April, 1989.

6. Jones, A. K. and Chapman, P. J., "CFD Combustion Modelling - A Comparison of Secondary Air System Designs," *Proc. TAPPI Eng. Conf.*, p. 559, 1992.

7. Siiskonen, P., Karvinen, R., Hyoty, P., Migaj, V. K., and Morgoun, A. V., "Combined Physical and Numerical Study of a Multilevel Air System," *Proc. Int'l Chem. Recovery Conf.*, p. 57, 1992.

8. Vakkilainen, E. K., Adams, T. N., and Horton, R. R., "The Effect of Recovery Furnace Bullnose Designs on Upper Furnace Flow and Temperature Profiles," *Proc. Int'l Chem. Recovery Conf.*, p. 101, 1992.

9. Adams, T. N. and Horton, R. R., "The Effects of Black Liquor Spray on Gas Phase Flows in a Recovery Boiler," *Proc. TAPPI Eng. Conf.*, p. 81, 1992.

10. Chapman, P. J., Janik, S. G., and Jones, A. K., "Visualization of the Recovery-Boiler Flow Fields Predicted by Computational Fluid Dynamics," *Tappi J.* 75(3), 133(1992).

11. Salcudean, M., Nowak, P., and Abdullah, Z., "Mathematical Modeling of Recovery Furnaces," *Proc. Int'l Chem. Recovery Conf.*, p. 197, 1992.

12. Abdullah, Z., Nowak, P., Salcudean, M., and Gartshore, I. S., "Investigation of Interlaced and Opposed Jet Arrangements for Recovery Furnaces," *Proc. TAPPI Eng. Conf.*, p. 103, 1992.

13. Quick, J. W., Gartshore, I. S., and Salcudean, M., "Interaction of Opposing Jets With Special Relevance to Recovery Furnaces," *Proc. TAPPI Eng. Conf.*, p. 123, 1992.

14. Chapman, P. J. and Jones, A. K., "Recovery Furnace Combustion Modeling Using Computational Fluid Dynamics," *Proc. Int'l Chem. Recovery Conf.*, p. 71, 1992.

15. Karvinen, R., Hyoty, P., and Siiskonen, P., "The Effect of Dry Solids Contents on Recovery Boiler Furnace Behavior," *Tappi J.* **74**(12), 171(1991).

16. Horton, R. R., Grace, T. M., and Adams, T. N., "The Effects of Black Liquor Spray Parameters on Combustion Behavior in Recovery Furnace Simulations," *Proc. Int'l Chem. Recovery Conf.*, p. 85, 1992.

17. Sutinen, J. E. and Karvinen, R., "Numerical Modeling of Char Bed Phenomena," *Proc. Int'l Chem. Recovery Conf.*, p. 79, 1992.

18. PreBFC User's Guide, Ver. 4.0, Fluent Inc., December 1991.

19. FLUENT User's Guide, Ver. 4.0, Fluent Inc., December 1991.

20. Launder, B. E. and Spalding, D. B., *The Numerical Computation of Turbulent Flows*, Imperial College of Science and Technology, London, 1973.

21. Incropera, F. P. and De Witt, D. P., *Fundamentals of Heat and Mass Transfer*, 2nd ed., John Wiley & Sons, New York, 1985.

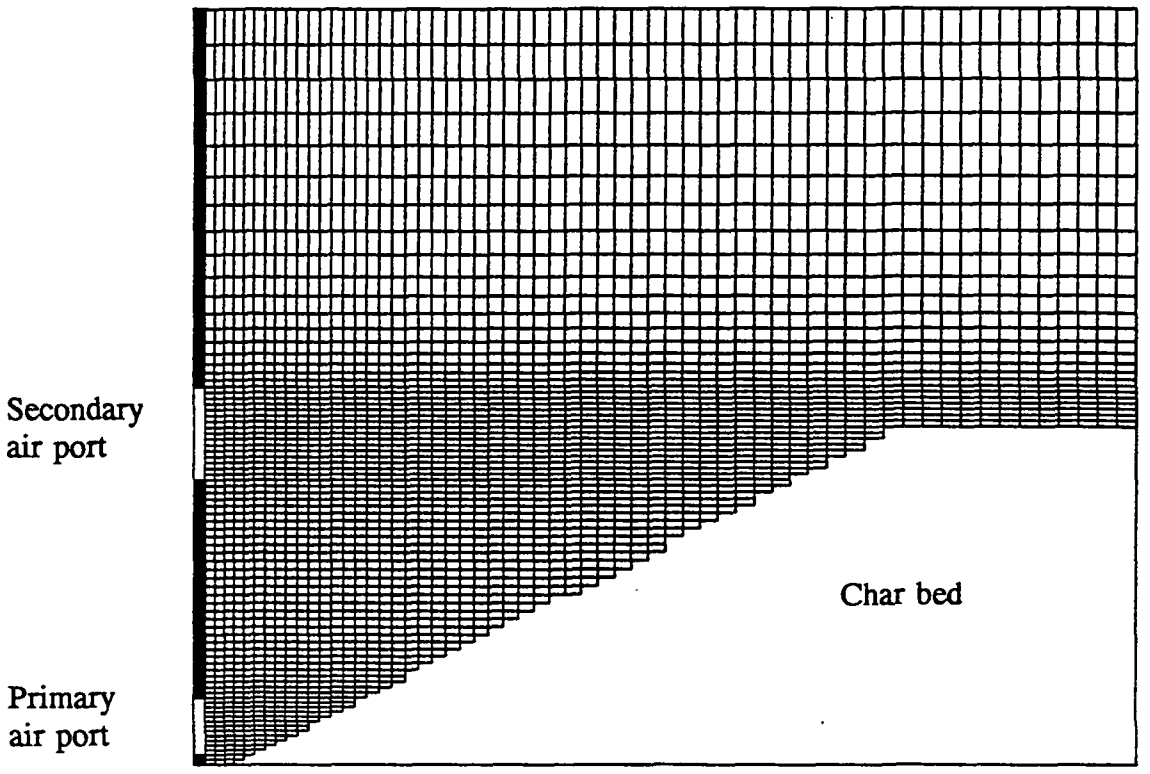

Figure 1. A Cartesian coordinate grid for a 2-D char bed model.

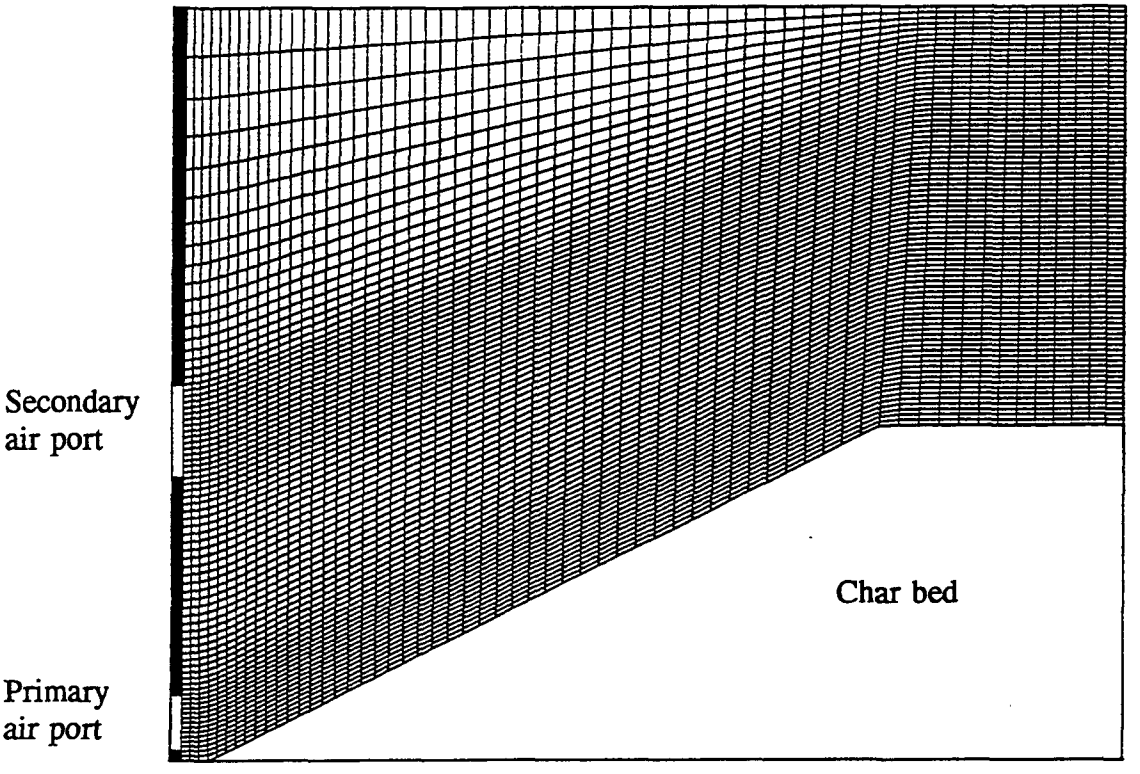

Figure 2. A BFC grid for a 2-D char bed model.

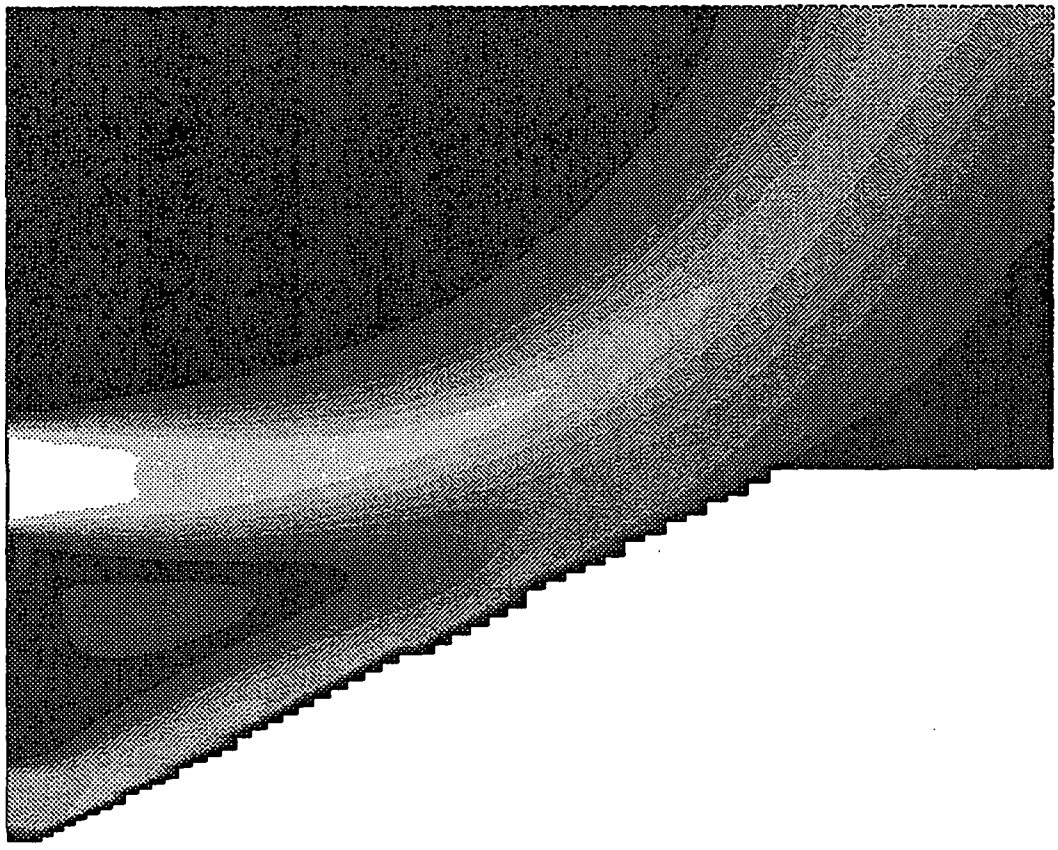

Figure 3. Velocity magnitude distribution for a step-bed model.

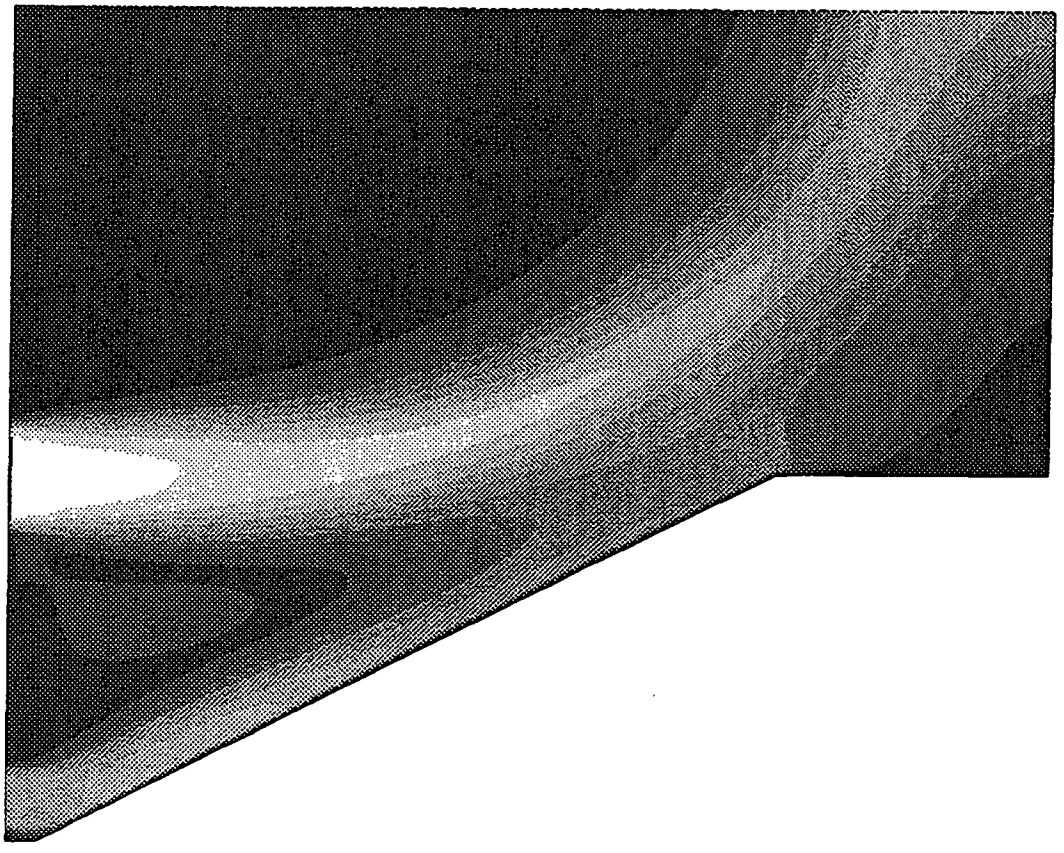

Figure 4. Velocity magnitude distribution for a smooth-bed model.

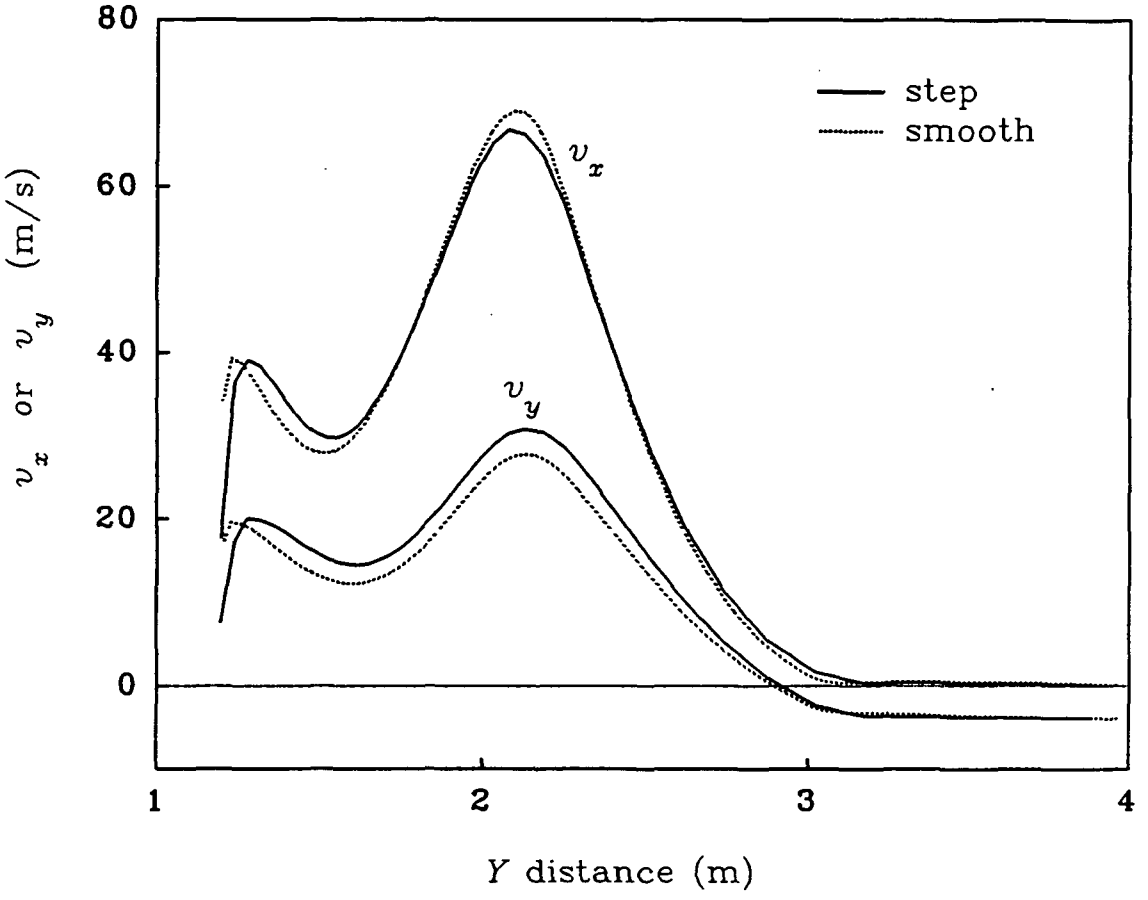

Figure 5. Comparison between velocity profiles of step bed and smooth bed along a vertical line at $x = 2.5$ m.

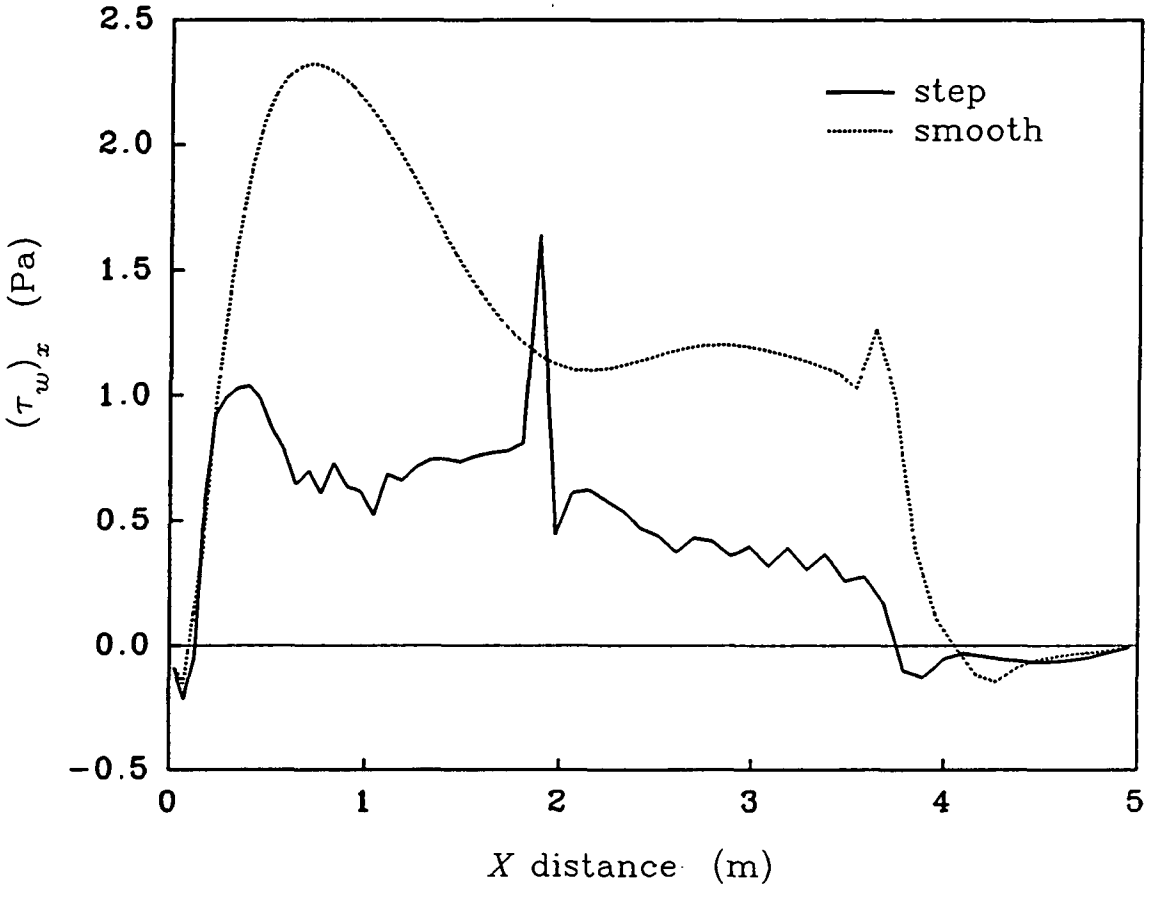

Figure 6. Comparison of shear stress distributions on step and smooth beds for isothermal cases.

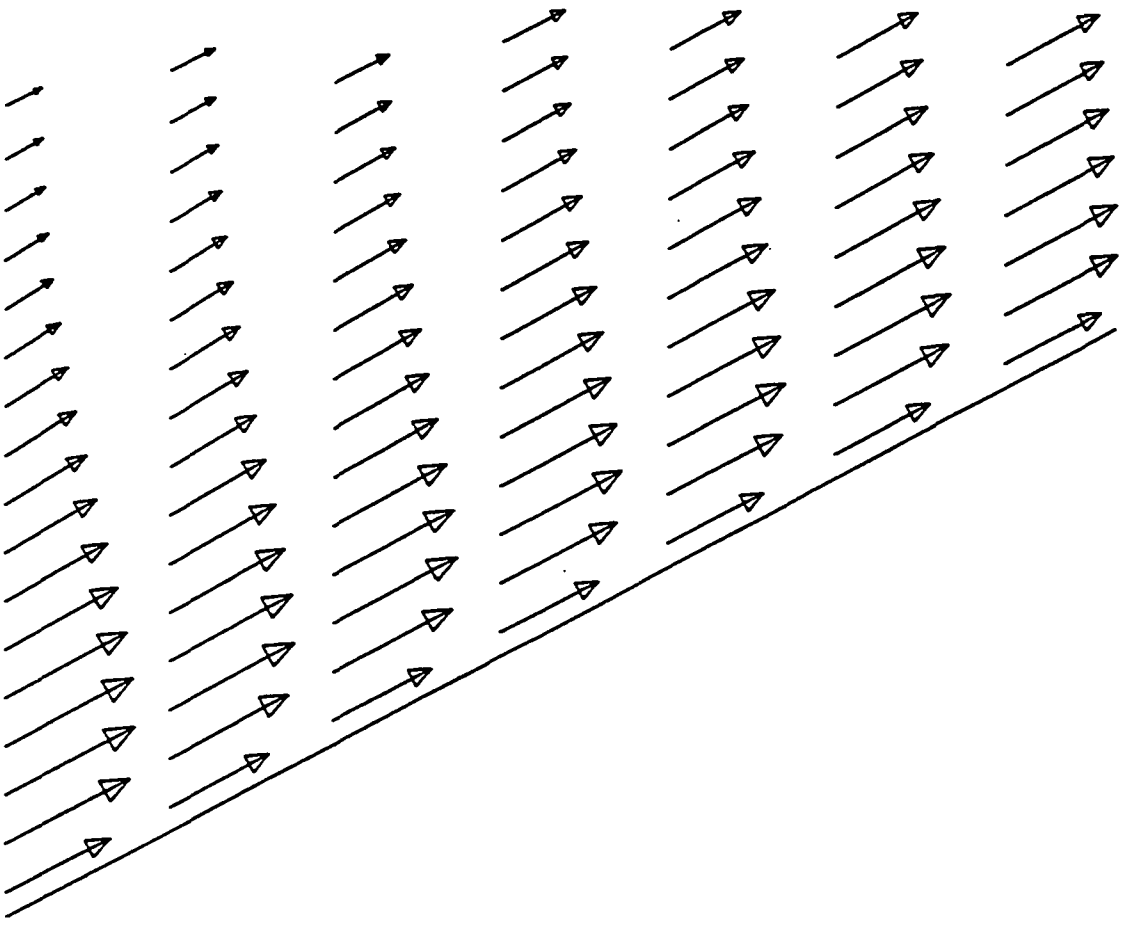

Figure 7. Velocity vectors near the smooth bed.

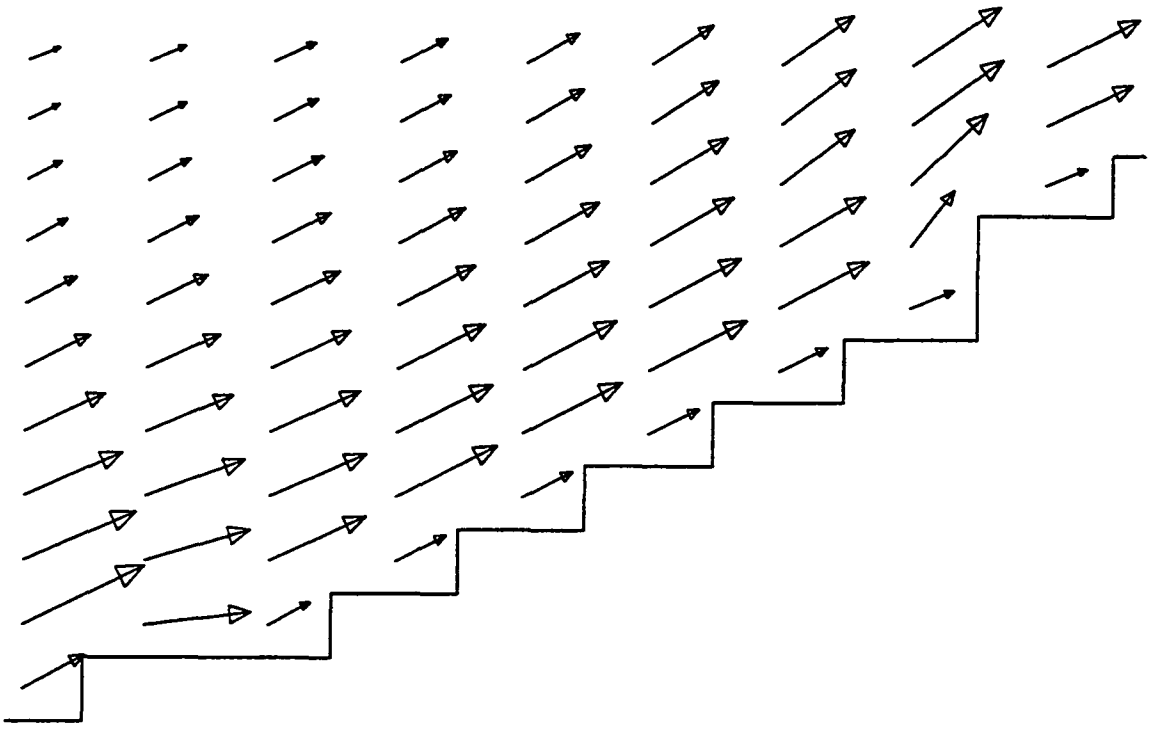

Figure 8. Velocity vectors near the step bed.

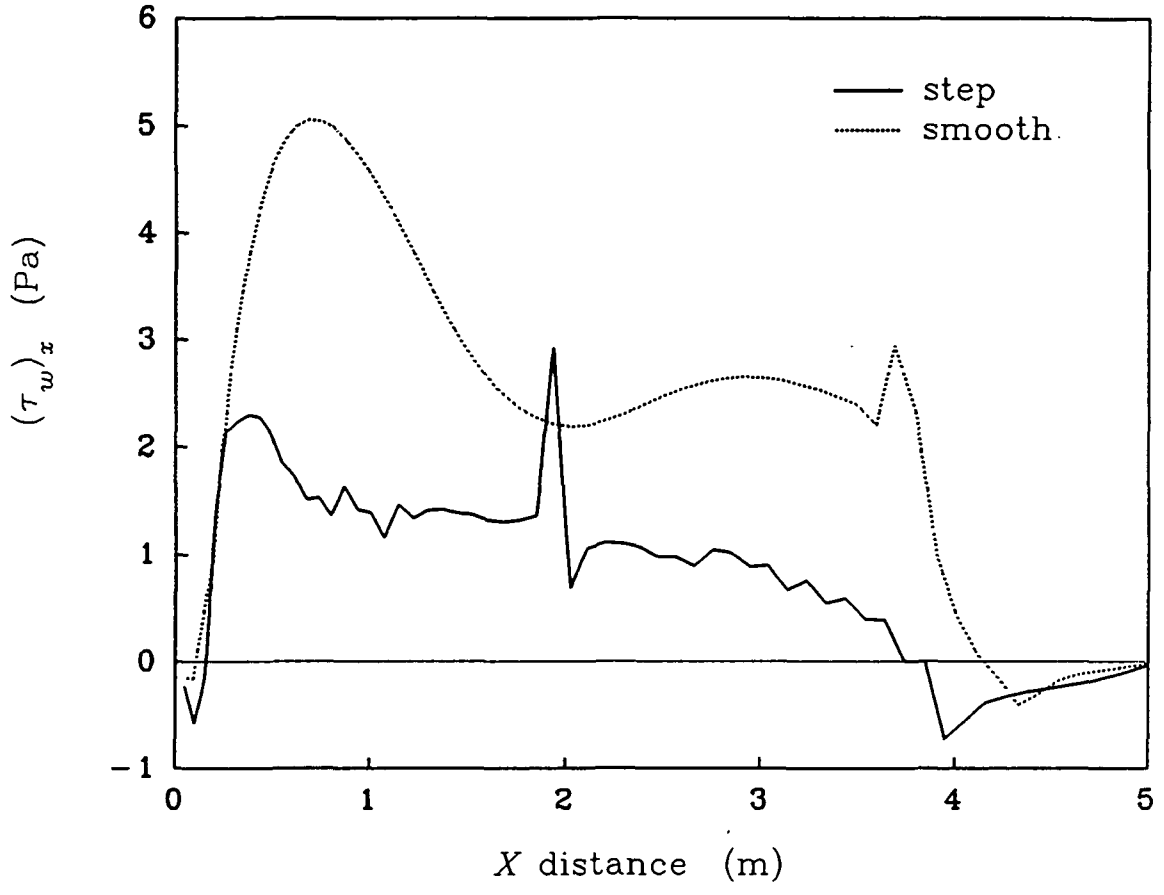

Figure 9. Comparison of shear stress distributions on step and smooth beds for nonisothermal cases.

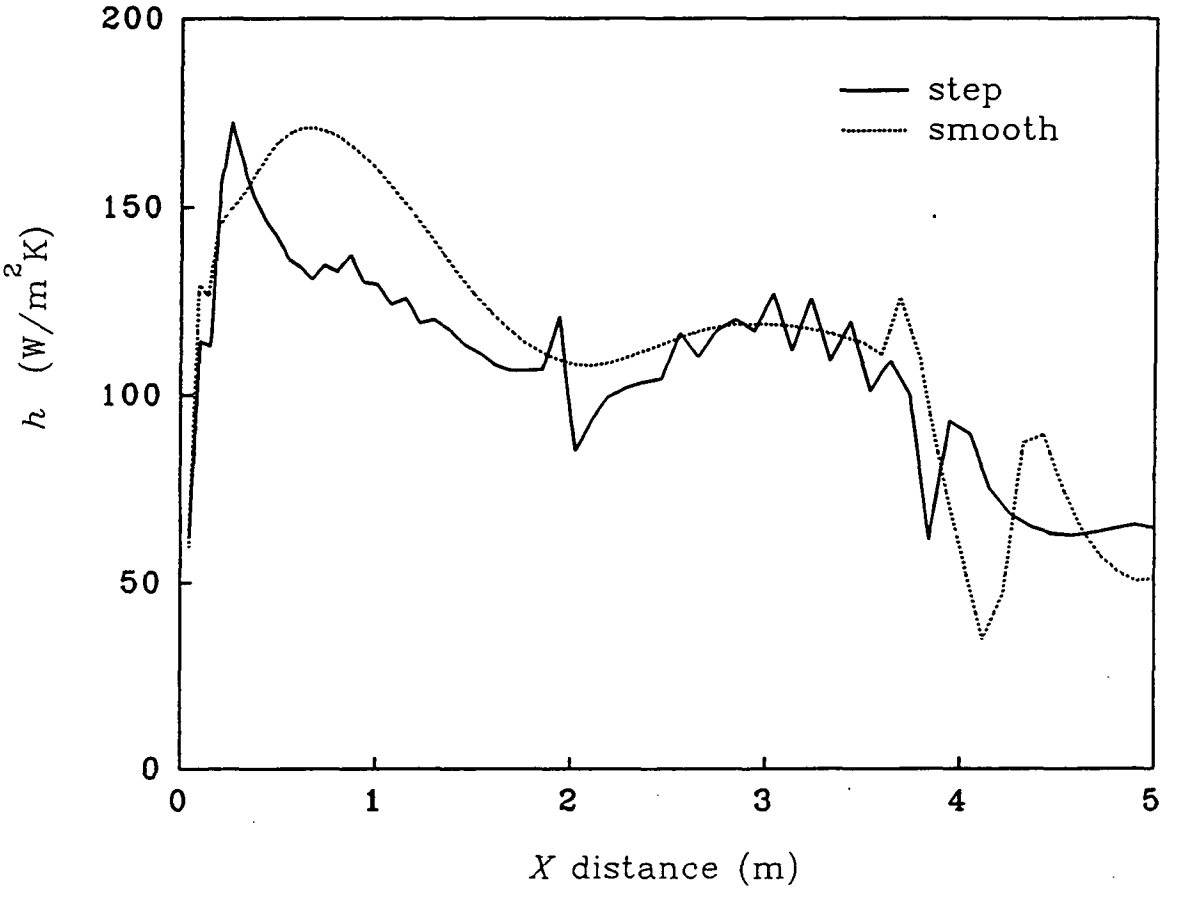

Figure 10. Heat transfer coefficients on step and smooth beds for nonisothermal cases.